Periodically driven quantum ratchets: Symmetries and resonances

S. Denisov,[1] L. Morales-Molina,[2] S. Flach,[2] and P. Hänggi[1]
[1]*Institut für Physik, Universität Augsburg, Universitätsstrasse 1, D-86135 Augsburg, Germany*
[2]*Max-Planck-Institut für Physik Komplexer Systeme, Nöthnitzer Strasse 38, 01187 Dresden, Germany*
(Received 16 March 2007; published 27 June 2007)

We study the quantum version of a tilting and flashing Hamiltonian ratchet, consisting of a periodic potential and a time-periodic driving field. The system dynamics is governed by a Floquet evolution matrix bearing the symmetry of the corresponding Hamiltonian. The dc-current appears due to the desymmetrization of Floquet eigenstates, which become transporting when all the relevant symmetries are violated. Those eigenstates that mostly contribute to a directed transport reside in phase space regions corresponding to classical resonances. Quantum dynamics leads to the dependence of the average velocity on the initial phase of the ac-field. A resonant enhancement (or suppression) of the dc-current, due to avoided crossings between different Floquet states, takes place upon tuning some control parameters. Our studies are predominantly aimed at experimental realizations of ac-driven quantum ratchets with cold atoms.

DOI: 10.1103/PhysRevA.75.063424 PACS number(s): 32.80.Pj, 05.45.Mt, 05.60.−k

I. INTRODUCTION

Ratchets are viewed as realizations of systems which produce a directed current from a fluctuating environment in the absence of gradients and net forces [1–5]. Initially proposed as an abstract physical model for the understanding of a micromolecular machinery [2], ratchet systems have found diverse applications in many areas [3–5], from mechanical devices [6] up to quantum systems [7–11]. Among the areas with growing interest is the study of ratchet dynamics for cold atoms [12]. Hamiltonian ratchets [13–17] with the corresponding symmetry predictions [13] have recently been successfully realized with cold rubidium and cesium atoms in optical lattices with a two-harmonics driving and a tunable weak dissipation [18]. In these experiments, the mechanism of the Sisyphus cooling [19] has been used in order to furnish initial conditions in the form of an *optical lattice*: an ensemble of atoms localized in the wells of a periodic potential created by laser beams. In the momentum space this corresponds to a narrow distribution near the momentum $p=0$. This is essential for the observation of the rectification effect, since the asymptotic current tends to zero for broad initial distributions in momentum space.

To describe the ratchet dynamics of the thermal cloud of cold atoms in optical lattices [18], a classical model has been used [13–15]. However, as the cloud of atoms in a far detuned optical potential [20] is cooled further down, one can obtain a system where quantum effects become relevant. Many studies of quantum ratchets are based on the kicked rotor model [7,16,21,22], which is readily treated numerically. In reality kicks may heat the system and degrade quantum effects. It is perhaps for that reason that other successful experiments [18] use a time continuous drive, which is also the choice in the present work.

The paper is organized as follows. In Sec. II we introduce the model for the quantum tilting ratchet and discuss its properties. The dynamics of the system is studied within the Floquet theory. We use the Husimi representation in order to link eigenstates to manifolds in the classical phase space. In Sec. III we study the relevant symmetries, whose violation leads to the directed current, and the desymmetrization mechanisms. Section IV is devoted to the dynamics of current rectification. We begin by discussing the dependence of the current on the initial condition. Then we investigate the appearance and controlling of quantum resonances that lead to a significant enhancement of directed transport. In Sec. V we introduce the realization of a quantum flashing ratchet system. Finally, in Sec. VI we summarize our results. Some of our important technical details are deferred to the Appendixes A–C.

II. MODEL SETUP

Let us start with a cloud of atoms, placed into a periodic potential (formed by an optical standing wave) and exposed to an external ac field. Assuming a low density, we neglect the interactions among the atoms. Hence our problem can be described by the Schrödinger equation

$$i\hbar\frac{\partial}{\partial t}|\psi(t)\rangle = H(t)|\psi(t)\rangle, \tag{1}$$

where the Hamiltonian H is of the form [18]

$$H(x,p,t) = \frac{p^2}{2} + [1+\cos(x)] - xE(t). \tag{2}$$

Here $E(t)$ is an external periodic field of zero mean, $E(t+T)=E(t)$, $\int_0^T E(t)dt=0$. We start the integration at initial time t_0.

The Hamiltonian (2) is periodic in time with period T. The solutions $|\psi(t+t_0)\rangle = U(t,t_0)|\psi(t_0)\rangle$ of the Schrödinger equation (1) can be characterized by the eigenfunctions of $U(T,t_0)$ which satisfy the Floquet theorem: $|\psi_\alpha(t)\rangle = e^{-i(E_\alpha/T)t}|\phi_\alpha(t)\rangle$, $|\phi_\alpha(t+T)\rangle = |\phi_\alpha(t)\rangle$. The quasienergies $E_\alpha(-\pi<E_\alpha<\pi)$ and the Floquet eigenstates can be obtained as solutions of the eigenvalue problem of the Floquet operator

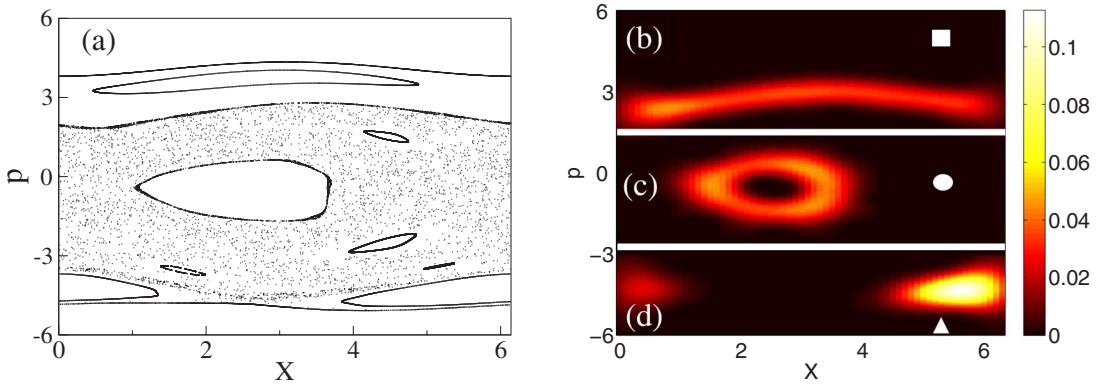

FIG. 1. (Color online) (a) Poincaré section for the classical limit and (b)–(d) Husimi representations for different Floquet eigenstates for the Hamiltonian (2) with $\hbar=0.2$ (momentum is in units of the recoil momentum, $p_r=\hbar k_L$, with $k_L=1$). The parameters are $E_1=E_2=2$, $\omega=2$, $\theta=-\pi/2$, and $t_0=0$.

$$U(T,t_0)|\psi_\alpha(t_0)\rangle = e^{-iE_\alpha}|\psi_\alpha(t_0)\rangle. \tag{3}$$

The Floquet eigenstates provide a complete orthonormal basis and the stroboscopic quantum state can be expressed as [23]

$$|\psi(mT,t_0)\rangle = \sum_\alpha C_\alpha(t_0)e^{-imE_\alpha}|\psi_\alpha(t_0)\rangle, \tag{4}$$

where the coefficients $\{C_\alpha\}$ depend on t_0. For later convenience the integer $\alpha=0,1,2,\ldots$, sorts the states $|\psi_\alpha\rangle$ such that the mean kinetic energy $\langle p^2\rangle_\alpha \equiv 1/T\int_0^T\langle\psi_\alpha|\hat{p}^2|\phi_\alpha\rangle dt_0$ monotonically increases. The "kinetic energy" defined here and throughout the text is two times the kinetic energy of the system.

By using the gauge transformation,

$$|\psi\rangle \to \exp\left[-\frac{i}{\hbar}x\left[\int_0^t E(t')dt' + I(0)\right]\right]|\psi\rangle,$$

where $I(t)$ is primitive of $E(t)$ with zero constant [24], we transform the original Hamiltonian (2) into a spatially periodic one (see Appendix A). Then the solution of the time-dependent Schrödinger equation for the new Hamiltonian may be written as

$$|\psi(t)\rangle = e^{-i/\hbar\int_0^t\{1/2[\hat{p}-A(t')]^2+(1+\cos x)\}dt'}|\psi(0)\rangle, \tag{5}$$

with the vector potential $A(t)=-\int_0^t E(t')dt'+A(0)$, where the constant $A(0)$ has to be chosen such that $\langle A(t)\rangle_T=0$ and $\langle\ldots\rangle_T$ stands for the time average over a period T. Due to discrete translational invariance and Bloch's theorem all Floquet states are characterized by a quasimomentum κ with $|\psi_\alpha(x+2\pi)\rangle=e^{i\hbar\kappa}|\psi_\alpha(x)\rangle$.

Here we choose $\kappa=0$ which corresponds to initial states where atoms equally populate all (or many) wells of the spatial potential. This allows us to use periodic boundary conditions for Eq. (1), with spatial period $L=2\pi$, so that the wave function can be expanded in the plane wave eigenbasis of the momentum operator $\hat{p}$, $|n\rangle=\frac{1}{\sqrt{2\pi}}e^{inx}$, viz.

$$|\psi(t)\rangle = \sum_{n=-N}^{N} c_n(t)|n\rangle. \tag{6}$$

A detailed discussion of the two numerical procedures used to integrate Eq. (1) is presented in Appendix B.

To examine the morphology of the quasienergy states we use the Husimi representation [25]

$$\rho(\langle x\rangle,\langle p\rangle) = \frac{1}{2\pi}|\langle\psi|\Phi_{\langle x\rangle,\langle p\rangle}\rangle|^2, \tag{7}$$

where

$$\Phi_{\langle x\rangle,\langle p\rangle}(x) = \frac{1}{(2\pi\sigma^2)^{1/4}}\exp\left\{-\frac{(\langle x\rangle-x)^2}{4\sigma^2}+i\langle p\rangle x/\hbar\right\} \tag{8}$$

with $\sigma=(\hbar/2)^{1/2}$. Here $\langle x\rangle$ and $\langle p\rangle$ stand for the average of the position and momentum, respectively. The Husimi representation provides an insightful, coarse grained description in the phase space [25].

III. RELEVANT SYMMETRIES AND THEIR VIOLATIONS

A. Classical limit

Let us briefly outline the classical case. In this limit the system is generically characterized by a nonintegrable dynamics with a mixed phase space containing both chaotic and regular areas in the three-dimensional phase space (x,p,t) [27]. Due to time and space periodicity of the classical equation of motion $\ddot{x}=-\frac{\partial H}{\partial x}$, we can map the original three-dimensional phase space onto a two-dimensional cylinder, $T^2=(x \bmod 1,p)$, by using the stroboscopic Poincaré section after each period $T=2\pi/\omega$, cf. Fig. 1(a). This provides a helpful visualization of the mixed phase space structure. A stochastic layer, located near the line $p=0$, originates from the destroyed separatrix of the undriven system, $E(t)=0$. The chaotic layer is confined by transporting Kolmogorov-Arnold-Moser-*tori*, which originate from perturbed trajectories of particles with large kinetic energies, $\langle p^2\rangle$. The stochastic layer is not uniform and contains different regular invariant manifolds—regular islands, unstable periodic orbits, and cantori [27].

There are two symmetries which need to be broken to fulfill the necessary conditions for the appearance of a dc-current $J=\lim_{t\to\infty}\frac{x}{t}=\langle\dot{x}\rangle$ [13]. If $E(t)$ is shift symmetric, i. e., $E(t)=-E(t+T/2)$, the symmetry

$$S_a:(x,p,t) \to (-x,-p,t+T/2) \tag{9}$$

is realized. Furthermore, if $E(t)$ is symmetric, i.e., $E(t+t_s)=E(-t+t_s)$ at some appropriate point t_s, the symmetry

$$S_b:(x,p,t) \to (x,-p,-t+2t_s) \tag{10}$$

holds. Any trajectory, when transformed using one of the above mentioned symmetry operations, yields again a trajectory of the system but with opposite velocity. Assuming that ergodicity holds in the stochastic layer (which means that all its average characteristics are independent on the initial conditions, and that symmetry-related trajectories have the same statistical weight, we conclude that the asymptotic velocity within the chaotic layer is zero. So, whenever S_a and/or S_b are realized, directed transport is forbidden inside the chaotic layer [13].

The two frequency driving,

$$E(t) = E_1 \cos(\omega t) + E_2 \cos(2\omega t + \theta), \tag{11}$$

ensures that for $E_1, E_2 \neq 0$ S_a is always violated. In addition S_b is violated for $\theta \neq 0, \pm\pi$. The appearance of a nonzero dc-current $J_{\mathrm{ch}}=\lim_{t\to\infty} 1/(t-t_0)\int_{t_0}^{t} p(t')dt'$ in this case is due to a desymmetrization of the chaotic layer structure [Fig. 1(a)]. It induces a desymmetrization of the events of directed motion to the right and left [28]. Due to ergodicity inside the layer, the asymptotic current is independent of the initial time t_0, for initial conditions located inside the chaotic layer. With the specific choice of the driving (11) it follows $J_{ch}(\theta) = -J_{ch}(-\theta)$ and $J_{ch}(\theta)=-J_{ch}(\theta+\pi)$ [13]. From perturbation theory it follows $J_{ch} \sim E_1^2 E_2 \sin\theta$ [13,14]. An efficient sum rule allows one to compute the average current J_{ch} by proper integration over the chaotic layer [16].

B. Quantum case

If the Hamiltonian is invariant under the shift symmetry S_a (9), then the Floquet operator possesses the property, see Eq. (179) in Ref. [23]:

$$U(T,t_0) = [U(T/2,t_0)^{\Upsilon}]^{\mathsf{T}} U(T/2,t_0). \tag{12}$$

Here U^{Υ} (seeing Appendix C) performs a transposition along the codiagonal of U. With Eq. (11) S_a is always violated.

Likewise, one can show that, if the Hamiltonian is invariant under the time reversal symmetry S_b (10), then the Floquet matrix has the property [29]

$$U(T,t_0) = U(T,t_0)^{\Upsilon}. \tag{13}$$

That symmetry will be recovered for $\theta=0,\pi$. More details about the derivation of the previous properties of the operator evolution are explained in Appendix C.

We introduce the quantum asymptotic current as the mean momentum expectation value

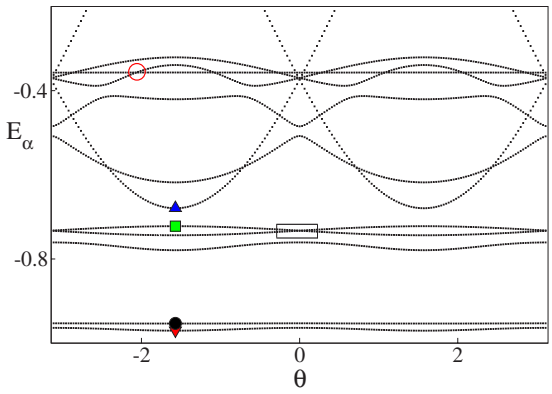

FIG. 2. (Color online) A part of the quasienergy spectrum as a function of the parameter θ. The symbols indicate the corresponding Floquet states shown in Figs. 1(b)–1(d). The empty (red) circle indicates the existence of an avoided crossing between two eigenstates. The empty square encloses the region of the spectrum that appears enlarged in Fig. 3.

$$J(t_0) = \langle \bar{p} \rangle_t = \lim_{t\to\infty} 1/(t-t_0) \int_{t_0}^{t} dt' \langle \psi(t',t_0)|\hat{p}|\psi(t',t_0)\rangle, \tag{14}$$

where $\bar{p}=\langle\psi|\hat{p}|\psi\rangle$ is the mean instantaneous momentum. Expanding the wave function in the Floquet basis the current becomes

$$J(t_0) = \sum_{\alpha} \langle p \rangle_{\alpha} |C_{\alpha}(t_0)|^2, \tag{15}$$

where $\langle p\rangle_{\alpha}$ is the mean momentum of the Floquet state $|\phi_{\alpha}\rangle$ (see Appendix D for more details). Thus we have to study the properties of Floquet states.

In general, the Floquet bands of the system [Eqs. (1) and (2)] depend on the control parameters like amplitudes, frequencies, and phase shifts of the components of the force $E(t)$. We vary the parameter θ while keeping the other fixed. In Fig. 2 we present the quasienergy bands as a function of θ. There are two remarkable features. First, the spectrum exhibits two symmetries, $E_{\alpha}(\theta)=E_{\alpha}(-\theta)$ and $E_{\alpha}(\theta)=E_{\alpha}(\theta+\pi)$, which are consequences of the choice (11). Second, while some bands show strong dispersion upon the variation of θ, reaching the maximal dispersion at $\theta=\pm\pi/2$, others have a rather flat dependence. In Figs. 1(b)–1(d) we present Husimi functions [25] for several Floquet states depicted by symbols in Fig. 2. The Planck constant $\hbar=0.2$ is in a range, where it is possible to establish a correspondence between different Floquet states and the invariant manifolds of the mixed phase space for the classical limit. The states (b)–(d) are located in various regular phase space regions.

On the other hand, from Fig. 2 we observe repulsion between some bands whereas others apparently cross each other. These crossings are in fact avoided crossings which lead to interesting effects.

For the symmetric case $\theta=0,\pm\pi$ the Floquet matrix has an irreducible representation using even and odd basis states $|n\rangle_{s,a}=(|n\rangle \pm |-n\rangle)/\sqrt{2-\delta_{n,0}}$. All the Floquet states appear as

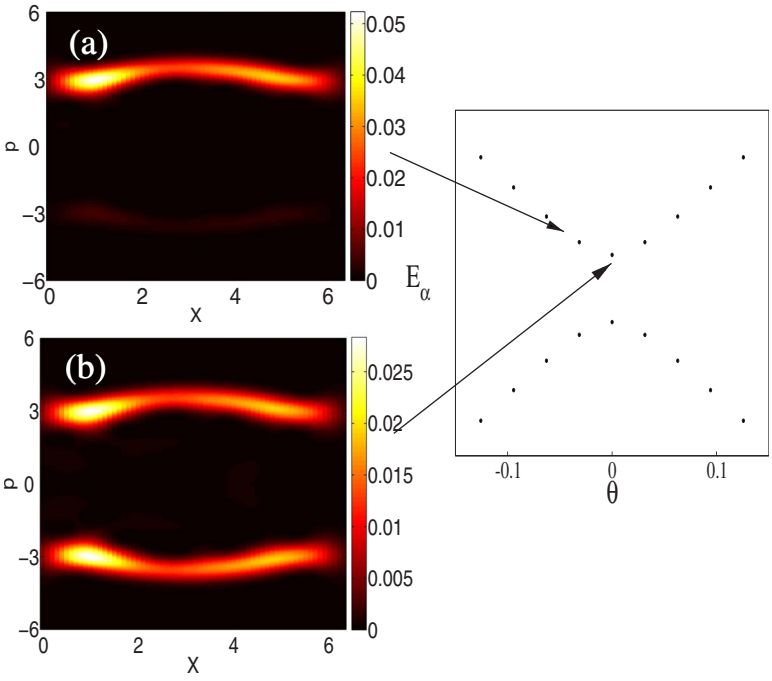

FIG. 3. (Color online) Right panel: Quasienergy spectrum in the vicinity of two quasidegenerated Floquet states. The symmetry is restored at the points $\theta=0,\pm\pi$ where the splitting is rather small. Left panels: Husimi function for different θ, (a) $\theta=-0.05$ and (b) $\theta=0$.

quasidegenerated doublets and $\langle p\rangle_\alpha=0$ for all α (see Figs. 2 and 3). We especially note that this is true for states with arbitrarily large kinetic energy, for which the corresponding quasienergies become almost pairwise degenerated. Consequently, following Eq. (15), $J=0$ in this case.

For $\theta\neq 0,\pm\pi$ the Floquet states become asymmetric and the quasidegeneracies are removed (Fig. 3). Floquet states acquire a nonzero mean momentum, thus becoming transporting. On the other hand, while in the symmetric case it is possible to have coherent tunneling oscillations between disconnected regular islands, in the nonsymmetric case a possible dynamical tunneling is suppressed [30]. Thus a wave packet initially located on a Floquet state with an asymmetric distribution of momentum [similar to the state shown in Fig. 3(b)] will undergo a permanent directional transport.

This phenomenon of desymmetrization results in a nontrivial dependence of the momentum upon θ. We can gain some understanding of this effect by modeling the evolution of two eigenstates, which form a parity-related pair at the point $\theta=0$, by neglecting their coupling with the rest of the states.

To this end, we take two eigenstates, Φ_a and Φ_b, which can be expanded in the plane wave basis $\pm|n\rangle$. The corresponding propagator for such a reduced system is

$$U_{ab}=\begin{pmatrix}1-\varepsilon & \Delta\\ \Delta & 1+\varepsilon\end{pmatrix}, \tag{16}$$

where the nondiagonal term Δ refers to the interaction between the states. In general, this quantity depends upon the momentum and driving field's characteristics, i.e., $\Delta=\Delta(p,E_1,E_2,\theta)$. On the other hand, the parameter ε breaks the parity symmetry, and yields $\varepsilon\sim nE_1^2E_2\sin\theta$ at a first-order of a perturbation theory. It is known that, in the absence of driving, $E(t)=0$, the asymptotic dependence of the splitting value on n is $\Delta\sim n^{-n}$, i.e., a superexponential decay [31].

The eigenstates in a plane-wave basis are

$$\Phi_s=\frac{1}{L(\gamma)}[1|n\rangle+(\gamma+\sqrt{1+\gamma^2})|-n\rangle], \tag{17}$$

$$\Phi_a=\frac{1}{L(\gamma)}[(\gamma+\sqrt{1+\gamma^2})|n\rangle-1|-n\rangle], \tag{18}$$

where $\gamma=\varepsilon/\Delta$ and $L(\gamma)=\sqrt{1+(\gamma+\sqrt{1+\gamma^2})^2}$. The symmetric case, $\theta=0$, corresponds to the limit $\gamma\to 0$. The eigenstate's momenta are

$$p_s\approx-\gamma n,\quad p_a\approx\gamma n. \tag{19}$$

At the opposite limit, $\gamma\to\infty$, we have

$$p_s\approx -n\left(1-\frac{1}{2\gamma^2}\right),\quad p_a\approx n\left(1-\frac{1}{2\gamma^2}\right). \tag{20}$$

For large n, Δ is small, but for $\epsilon=0$ (symmetric case) it follows $\gamma=0$, and the eigenstates carry zero momentum. Deviating from $\theta=0$, the moments quickly reach values $\pm n$. That happens for $E_1^2E_2\sin\theta\gg n^{-n-1}$, which will hold for any nonzero E_1, E_2, θ, provided n is large enough.

Leaving the region corresponding to the chaotic layer, the splitting between the doublets drops quite suddenly to zero. This explains the momentum asymmetry in Fig. 3 for values of θ slightly deviated from $\theta=0$.

IV. AVERAGE CURRENT AND RESONANCES IN CURRENT RECTIFICATION

The asymptotic current (14) depends on the initial conditions, and, following Eq. (15), only those Floquet states which overlap with the initial wave function, $\psi(t_0)$, contrib-

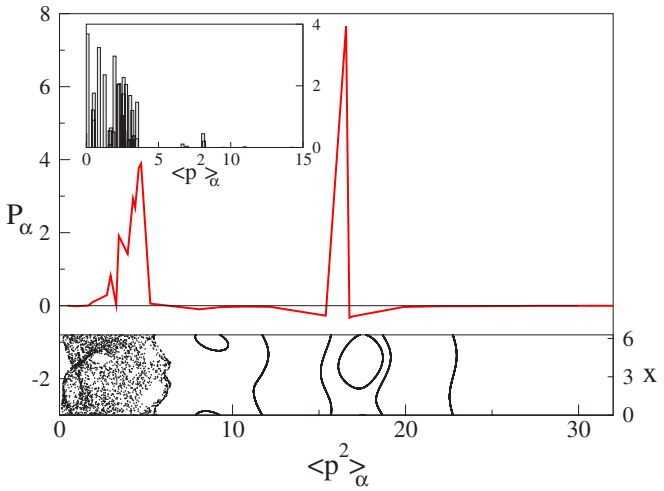

FIG. 4. (Color online) Top: The line corresponds to the cumulative momentum, P_α (see text). All the momenta are given in units of the recoil momentum p_r. Inset: The bars depict the weights of the respective Floquet states that overlap with the initial state $|0\rangle$. The bars have been multiplied by a factor of 10. Bottom: The plot of the average kinetic energy, complementary to the Poincaré section in Fig. 1(a). Starting from an initial point $(x(t_0),p(t_0))$, we calculate the kinetic energy averaged over one period, $E_{kin}(mT) = \frac{1}{T}\int_{t_0+(m-1)T}^{t_0+mT} p^2(t)dt$, and consequently plot points $(x(mT),E_{kin}(mT))$. The parameters are the same as in Fig. 1.

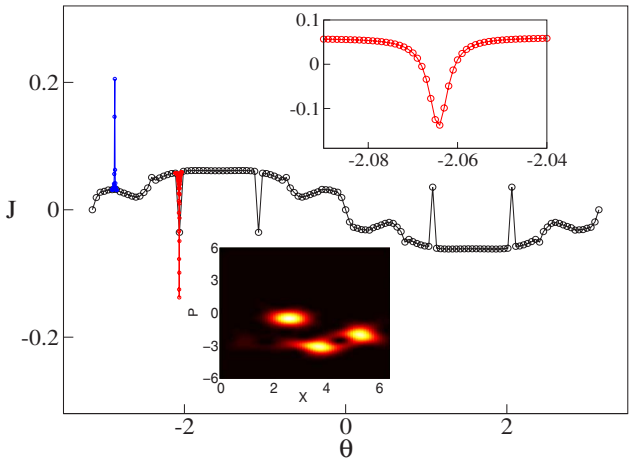

FIG. 5. (Color online) The average current J (in units of the recoil momentum) vs θ. Blue and red delta points are obtained with higher resolution, in particular θ regions. Insets: (top right) Enlargement of the region around $\theta=-2.06$. (bottom) Husimi function for the eigenstates in the avoided crossing indicated in Fig. 2.

ute to its subsequent time evolution. From now on, we restrict our analysis to the initial condition in the form of a plane wave with wave vector $n=0$, i.e., $\psi(t_0)=|0\rangle=\frac{1}{\sqrt{2\pi}}$. This initial condition spreads over Floquet states with low kinetic energies, namely over those eigenstates for which the Husimi representations lie in the chaotic layer's region (Fig. 4).

In the previous section we have discussed the mechanism of the desymetrization when we tuned the system away from the symmetry point $\theta=0$. In order to estimate a dc-current value we need qualitative information about mean momentum values acquired by Floquet states. As a suitable quantity to study this issue, we use the cumulative average momentum, $P_\alpha=\Sigma_{s\leq\alpha}\langle p\rangle_\alpha$. Figure 4 depicts the cumulative average momentum, obtained from the recursive relation $P_{\alpha+2}=P_\alpha+\langle p\rangle_{\alpha+1}+\langle p\rangle_{\alpha+2}$, with $P_0=\langle p\rangle_0$ [26]. The asymmetry stems mainly from Floquet states located in the chaotic layer region of the classical phase space. The dependence has several peaks. The Floquet states with higher values of the mean momentum, which yields strong dc-currents, are located at kinetic energy's regions that correspond to classical transporting resonance islands (see bottom part of Fig. 4). A more detailed analysis by using the Husimi distribution confirms this finding. There are infinitely many high-order resonance islands in the phase space of the Hamiltonian system (2) [27] whose sizes shrink quickly as the resonance's order increases with $\langle p^2\rangle\to\infty$. The desymmetrization effect is observable only when a resonance island can host more than one Floquet state. With increasing $\langle p^2\rangle_\alpha$, P_α approaches zero in full accordance with the fact that total current over the whole momentum space should be zero [16].

The asymptotic current for a fixed initial condition $|\psi(t_0)\rangle$ depends in general on the initial time t_0. Note that this is possible also in the classical case, since the initial distribution may overlap with different regular transporting manifolds [16]. However, if we start with a cloud of particles located exactly inside the chaotic layer, the classical asymptotic current will be independent of t_0 for any choice of the distribution function over the chaotic manifold. This is not true for the quantum case where the current may even change its sign with the variation of t_0. It is a consequence of the linear character of the Schrödinger equation [32]. We will first discuss the results obtained after averaging over the initial time t_0. Then we can assign a unique current value, $J=1/T\int_0^T J(t_0)dt_0$, for fixed parameters of the ac-field, E_1, E_2, and θ. Figure 5 shows the dependence of the average current on the asymmetry parameter θ for the initial condition $|\psi\rangle=|0\rangle$. The average current J shows the expected symmetry properties $J(\theta)=-J(\theta+\pi)=-J(-\theta)$. These symmetries for the current imply that the results obtained for the interval $(-\pi,-\pi/2)$ hold for other intervals as well.

The typical dependence of the average current J on θ is shown in Fig. 5. The curve presents a smooth profile with several peaks. By comparing Fig. 5 with the quasienergy spectrum Fig. 2, one can associate peaks with single sharp avoided crossings (resonances) between two Floquet eigenstates.

The Husimi function gives us additional insights for the appearance of these peaks (see insets in Fig. 5). It shows two states that are located in the chaotic layer, one of them near $p=0$, while the other is off the line $p=0$ with a strong asymmetry in momentum, corresponding to a regular transporting manifold. Off resonance the initial zero-plane wave state mainly overlaps with the first eigenstate, which yields some nonzero current due to desymmetrization. At resonance this eigenstate mixes with the "transporting" one, resulting in a strong enhancement of the current which is reflected in the presence of peaks.

From an experimental point of view a too narrow resonance may become undetectable due to resolution limitations. We thus studied how to vary the width of the reso-

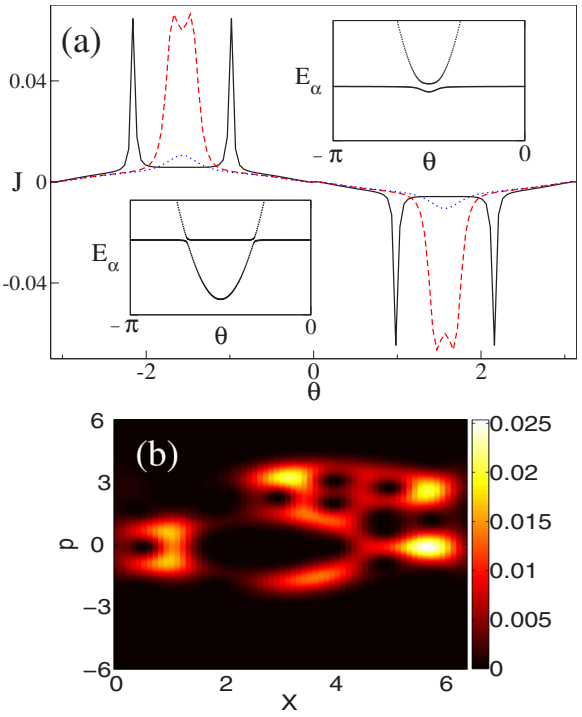

FIG. 6. (Color online) (a) The average current J (in units of the recoil momentum) vs θ for different amplitude values of the second harmonic, E_2: 0.95 (pointed line), 1 (dashed line), and 1.2 (solid line). Insets: relevant details of the quasienergy spectrum versus θ in the resonance region for $E_2=1$ (top right) and $E_2=1.2$ (bottom left). The parameters are $E_1=3.26$ and $\omega=3$. (b) Husimi function for the upper eigenstate that appears in (a) (top right inset) with $\theta=-\pi/2$.

nance without much affecting its amplitude. It turns out to be possible by tuning another control parameter, e.g., the amplitude E_2. We decrease this field amplitude in order to disentangle the two Floquet states and remove the avoided crossing. That will happen for some value of E_2 at $\theta=\pm\pi/2$. The details of the quasienergy spectrum around that critical point are shown in the insets in Fig. 6(a). The two quasienergy spectra disentangle for $E_2=1$ but stay close over a sufficient broader range of θ values. Thus the resonances become broader, as seen in Fig. 6(a). A further decrease of E_2 to a value of 0.95 leads to a strong separation of the two spectra, and consequently to a fast decay of the amplitude of the resonance.

As we already know, in resonance Floquet states mix. Here the new eigenstate contains contributions both from the original chaotic state as well as from the regular transporting island state (see Fig. 6). The Husimi distribution of this mixed state shows strong asymmetry as expected. The states from the chaotic sea and the regular transporting island are connected by a narrow isthmus. Therefore it is possible to leak from the nontransporting to the transporting island, which, in principle, should reduce significantly the observation time for the detection of resonances. It was shown in [28], for the classical limit, that for a maximum desymmetrization of the phase space, particles may stick to a regular island leading to a ballistic flight. Hence, based on the classical analog, we can say that our hybrid state serves as a quantum ballistic channel.

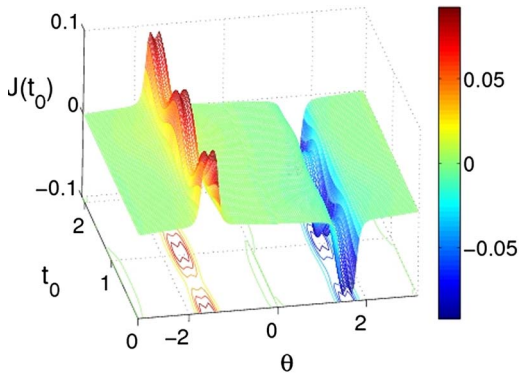

FIG. 7. (Color online) Current dependence on the initial time t_0 and θ. The parameters are the same as in Fig. 6. The current is in units of the recoil momentum, $p_r=\hbar k_L$.

On the other hand, as already mentioned, the asymptotic current depends on the initial time t_0. The observed resonance structures, due to resonant interaction between Floquet states (avoided crossings of quasienergies), are independent of the initial time t_0. In Fig. 7 we plot the nonaveraged current as a function of both θ and t_0. While the smooth background is barely resolvable with the naked eye, the resonances are clearly seen, and their position is not depending on t_0, while their amplitude does. That implies that one can further maximize the resonant current by choosing properly the initial values for t_0.

So far, we have considered only the frequencies, $\omega=2$ and 3 (Figs. 1–7). To gain a better understanding of the resonances, we compute the dependence of the current as a function of the frequency of the driving force (see Fig. 8). This figure shows the appearance of peaks, whose amplitudes increase as the frequency decreases. However, for larger frequencies, peaks show up for specific frequencies, a result which depends on the drive amplitudes. Interestingly, one can notice the inversion of current.

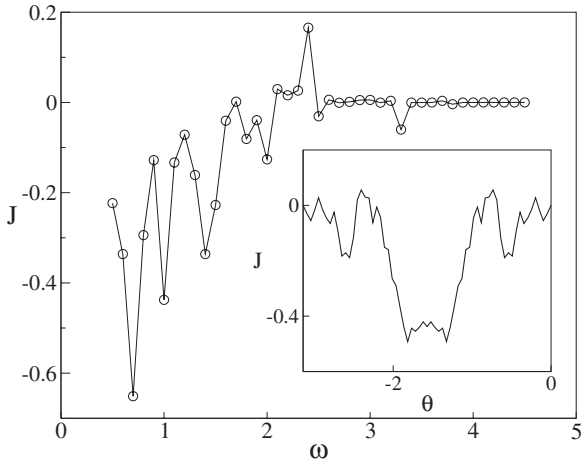

FIG. 8. The average of current J (in units of the recoil momentum) versus frequency ω of the driving force for $\theta=-\pi/2$. Inset: The average of current J versus θ for $\omega=1$. The plot of the current is depicted for the interval $(-\pi/2,0)$, since the current is antisymmetric with respect to a reflection at the origin. The other parameters are $E_1=3$ and $E_2=1.5$.

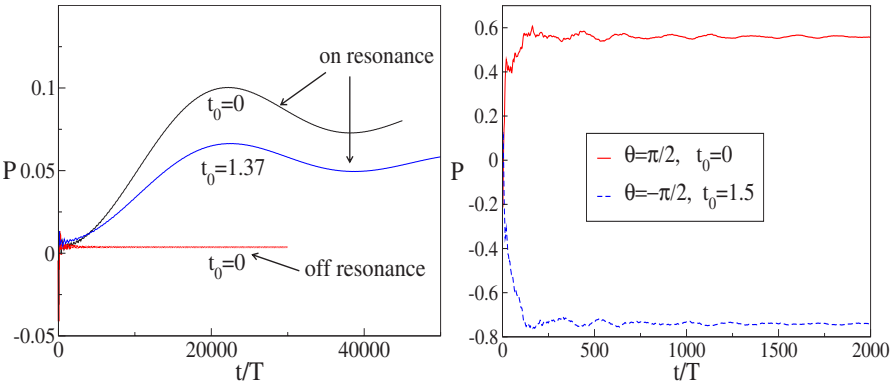

FIG. 9. (Color online) Momentum (in units of the recoil momentum) of state $|0\rangle$ as a function of time (in units of periods). Left panel: On resonance cases $\theta=-\pi/2$ for different t_0. Off resonance case $\theta=-2.2$. The parameters are $\omega=3$, and $E_1=3.26$, $E_2=1$. Right panel: Case $\omega=1$ with parameters $E_1=3$ and $E_2=1.5$.

In order to increase the current, we reduce the frequency of the ac-force $E(t)$. The asymptotic current for $\omega=1$ is shown in the inset of Fig. 8. We again observe a clear broad resonance, but the maximum current value increases by an order of magnitude up to 0.5 in units of recoil momenta.

Real experiments are always limited by a finite observation time. Therefore the rate of convergence to the asymptotic current value, Eq. (12), becomes a crucial issue. To give a more realistic approach of our above results to experiments, we perform numerical computations using the running average momentum (current) definition,

$$P = \frac{1}{t}\int_0^t \bar{p}dt. \tag{21}$$

The time evolution for the instantaneous momentum $P(t)$ is shown in Fig. 9. The top of Fig. 9 shows that off resonance the momentum rapidly evolves towards an asymptotic value, while in resonance the momentum performs long term oscillations which slowly approach the asymptotic value as the time increases. To speed up the convergence of the momentum towards the asymptotic value, we reduce the frequency. Figure 9 shows large currents close to the recoil momentum with relaxation times of the order of 100–200 periods for $\omega=1$. The above results were obtained for $\hbar=0.2$. We have repeated the calculations using $\hbar\sim 1$ and observed similar results.

V. QUANTUM HAMILTONIAN RATCHETS WITH FLASHING POTENTIALS

Recent experiments have shown the possibility to achieve an optical lattice with variable asymmetry [33].

The Hamiltonian in this case is given by

$$H(x,p,t) = \frac{p^2}{2} + U(x)E(t), \tag{22}$$

where $U(x+L)=U(x)$ and $E(t+T)=E(t)$.

Here, we take, as in [33], the potential

$$U(x) = K[\cos(x) + s\cos(2x+\theta_p)], \tag{23}$$

where θ is the parameter which makes the potential asymmetric for values different from $0,\pm\pi$. The relevant symmetries for the classical limit of the Hamiltonian (22) are

$$\mathcal{S}_1:(x,p,t) \to (-x+2x_s,-p,t)$$

$$\text{if} \quad U(x+x_s) = U(-x+x_s) \quad \text{for some } x_s, \tag{24}$$

$$\mathcal{S}_2:(x,p,t) \to (x,-p,-t+2t_s)$$

$$\text{if} \quad E(t+t_s) = E(-t+t_s) \quad \text{for some } t_s, \tag{25}$$

$$\mathcal{S}_3:(x,p,t) \to (-x+2x_s,-p,t+T/2)$$

$$\text{if} \quad E(t) = -E(t+T/2) \text{ and } U(x+x_s) = -U(-x+x_s), \tag{26}$$

$$\mathcal{S}_4:(x,p,t) \to (x+L/2,-p,-t+2t_s)$$

$$\text{if} \quad E(t+t_s) = -E(-t+t_s) \text{ and } U(x) = -U(x+L/2). \tag{27}$$

It is easy to see that a two-harmonic potential Eq. (23) is insufficient to break the time-reversal symmetry $\mathcal{S}_2$ (25). Thus an asymmetric ac-modulated function $E(t)$ is needed to desymmetrize the system. We use the two-harmonic function (11), which ensures that for $\theta_p \neq 0,\pm\pi$ and $\theta \neq 0,\pm\pi$ all the relevant symmetries, Eqs. (24)–(27), are violated. As stated before the quantum system inherits the same symmetries as the classical limit. Therefore a current should appear as the symmetries are broken.

Figure 10 shows the average current J versus θ for the asymmetric potential, $\theta_p=-\pi/2$, at strong quantum limit $\hbar=1$. Since the current dependence possesses the symmetry $J(\theta)=-J(\theta+\pi)=-J(-\theta)$, it is sufficient to plot the current for the interval $\theta\in(-\pi,0)$. As for the case of rocking ratchets, we found evidence for quantum resonances and dependence of the asymptotic current on the initial time t_0 (see inset in Fig. 10).

VI. CONCLUDING REMARKS

In summary, we have investigated the mechanisms of the emergence of an average current in ac-driven quantum systems. The key mechanism of the current rectification is the desymmetrization of Floquet states. A peculiarity of the quantum ratchet is its strong dependence of the current on the chosen initial time t_0 of the applied field. We identified quantum resonances induced by avoided crossings between

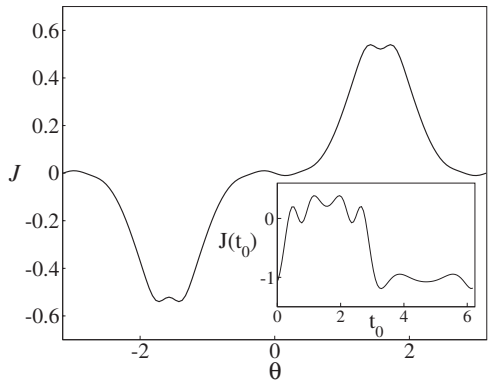

FIG. 10. The average current J (in units of the recoil momentum) vs θ. Inset: Asymptotic current as a function of the initial condition t_0 at $\theta=-\pi/2$. The parameters are $E_1=2$, $E_2=1.5$, $\hbar=1$, and $\omega=1$, $K=1.5$, $s=0.25$, and $\theta_p=-\pi/2$.

Floquet states which enhance the current drastically. Optimizing the drive frequency, amplitude, and initial phase, resonant currents easily reach the recoil momentum value and should be experimentally observable using driven cold atoms in optical lattices [18,33].

ACKNOWLEDGMENT

This work has been supported by the DFG Grant No. HA1517/31-1 (P.H. and S.F.).

APPENDIX A: GAUGE TRANSFORMATION: SOME RELEVANT QUANTITIES

We introduce the transformation

$$|\tilde{\psi}\rangle = \exp\left[\frac{i}{\hbar}xA(t)\right]|\psi\rangle$$

with $A(t)=-(E_1/\omega)\sin(\omega t)-(E_2/2\omega)\sin(2\omega t+\theta)$.

Substituting into Eq. (1) we can rewrite the Schrödinger equation as

$$i\hbar\frac{\partial}{\partial t}|\tilde{\psi}(t)\rangle = \tilde{H}(t)|\tilde{\psi}(t)\rangle, \tag{A1}$$

where $\tilde{H}(t)=\frac{1}{2}[\hat{p}-A(t)]^2+[1+\cos(x)]$.

To compute the momentum we start from the definition

$$\tilde{p}(t) = \left\langle \tilde{\psi}\left| -i\hbar\frac{\partial}{\partial x}\right|\tilde{\psi}\right\rangle = -i\hbar\int_{-\infty}^{\infty}\tilde{\psi}^*\frac{\partial}{\partial x}\tilde{\psi}dx = p(t)+A(t), \tag{A2}$$

where $\langle\tilde{p}\rangle_T=\langle p\rangle_T$.

The kinetic energy $\mathcal{T}$ is given by

$$\mathcal{T}(t) = \langle\psi|\hat{p}^2|\psi\rangle = \langle\psi|-\hbar^2\frac{\partial^2}{\partial x^2}|\psi\rangle$$
$$= \left\langle \exp\left[\frac{i}{\hbar}xA(t)\right]\tilde{\psi}\left| -\hbar^2\frac{\partial^2}{\partial x^2}\right|\exp\left[-\frac{i}{\hbar}xA(t)\right]\tilde{\psi}\right\rangle. \tag{A3}$$

After straightforward calculations

$$\mathcal{T}(t) = \tilde{\mathcal{T}}(t) - 2A(t)\tilde{p}(t) + A(t)^2. \tag{A4}$$

The average kinetic energy reads

$$\langle\mathcal{T}\rangle_T = \langle\tilde{\mathcal{T}}\rangle_T - 2\langle A(t)\tilde{p}(t)\rangle_T + \langle A(t)^2\rangle_T. \tag{A5}$$

Recalling the Husimi distribution,

$$\rho(\langle x\rangle,\langle p\rangle) = \frac{1}{2\pi}|\langle\psi|\Phi_{\langle x\rangle,\langle p\rangle}\rangle|^2, \tag{A6}$$

we can recast it in the new frame of variables as

$$\tilde{\rho}(\langle x\rangle,\langle p\rangle) = \frac{1}{2\pi}\left|\int_{-\infty}^{\infty}e^{-ixA(t)/\hbar}\psi^*(x,t)\times e^{ix\langle p\rangle/\hbar+(\langle x\rangle-x)^2/4\sigma^2}dx\right|^2,$$

$$\frac{1}{2\pi}\left|\int_{-\infty}^{\infty}\psi^*(x,t)e^{ix[\langle p\rangle-A(t)]/\hbar+(\langle x\rangle-x)^2/4\sigma^2}dx\right|^2 = \rho\{\langle x\rangle,\langle p\rangle-A(t)\}. \tag{A7}$$

Finally, after reversing the operations, we find

$$\rho(\langle x\rangle,\langle p\rangle) = \tilde{\rho}\{\langle x\rangle,\langle p\rangle+A(t)\}. \tag{A8}$$

APPENDIX B: NUMERICAL INTEGRATION SCHEMES

In order to find the numerical solution for the time-dependent Schrödinger equation we have used two different methods of integration. The first method has been described in [34]. It starts by using the expansion Eq. (6) and approximating

$$\hat{A}(t) = \frac{\Delta t}{\hbar}A(t)\sum_k\delta(t-k\Delta t) \tag{B1}$$

for the time dependence of the vector potential $A(t)=-(E_1/\omega)\sin(\omega t)-(E_2/2\omega)\sin(2\omega t+\theta)$, with $\Delta t=2\pi/(\omega N_t)$, where N_t is the number of integration steps per period.

The integration is carried out computing the coefficients $c_n(t_k+\Delta t)$ $(t_k=k\Delta t)$ by successive multiplication of the vector $\mathbf{c}(t_k)$ by a unitary matrix

$$\mathbf{c}(t_k+\Delta t) = \mathbf{UQVQ}^{-1}\mathbf{c}(t_k) \tag{B2}$$

where U and V are diagonal matrices with

$$U_{n,n} = \exp\left\{-i\hbar\frac{\Delta t}{2}\left[n^2-2n\frac{A(t)}{\hbar}+\frac{A(t)^2}{\hbar^2}\right]\right\} \tag{B3}$$

and $V_{n,n}=\exp(-i\Delta t\tilde{v}_n)$.

$\tilde{v}_n$ are the eigenvalues of the matrix representation $\mathbf{M}$ of the operator $(1/\hbar)\cos(\hat{x})$. $\mathbf{Q}$ is an orthogonal (unitary) matrix that transforms $\mathbf{M}$ into diagonal form ($\mathbf{M}=\mathbf{Q}\tilde{\mathbf{V}}\mathbf{Q}^{-1}$). $\tilde{\mathbf{V}}$ is a diagonal matrix with elements $\tilde{v}_n$.

The symmetric matrix $\mathbf{M}$ has the structure $M_{n,m}=(\delta_{m,n+1}+\delta_{m,n-1})/(2\hbar)$. This method permits one to decrease the number of steps per period [35]. Nevertheless, it involves several matrix products and therefore its efficiency is degraded.

To check our results we use a second integration method which is more efficient [29]. We expand again over plane waves but this time we write down the expansion coefficients as a product of two time dependent functions, viz.

$$|\psi(t)\rangle = \sum_{n=-N}^{N} a_n(t)\phi_n(t)|n\rangle. \tag{B4}$$

Assuming that $\phi(t)$ is a solution of the problem

$$i\hbar\partial_t\phi_n(t) = \frac{\hbar^2}{2}\left[n - \frac{A(t)}{\hbar}\right]^2\phi(t), \tag{B5}$$

we obtain for $\phi_n(t)$ the solution

$$\phi_n(t) = \exp\left\{-i\frac{\hbar}{2}\left[n^2 t - \frac{2n}{\hbar}\int_0^t A(t')dt' + \frac{1}{\hbar^2}\int_0^t A(t')^2 dt'\right]\right\}. \tag{B6}$$

Then inserting Eq. (B4) into Eq. (A1) we obtain the set of equations for the amplitudes $a_n(t)$,

$$\dot{a}_n = -i\frac{1}{2\hbar}\left[\frac{\phi_{n+1}^t}{\phi_n^t}a_{n+1} + \frac{\phi_{n-1}^t}{\phi_n^t}a_{n-1}\right]. \tag{B7}$$

To obtain the propagator $U(T,0)$, we start with the initial states $a_n^k(0)=\delta_{n,k}$, where $-N\leqslant n,k\leqslant N$ and integrate over one time period T. Here the kth column of the matrix for the propagator is given by $a_n^k(T)\phi_n^k(T)$. For the computation we have neglected the contribution originating from $A^2(t)$ and the constant term $1/\hbar$ in the potential since they only yield global phase factors.

APPENDIX C: SYMMETRIES OF FLOQUET OPERATOR

Let us first analyze the time reversal symmetry:

$$S_b: t \to -t, \quad x \to -x.$$

In the momentum representation basis, $|n\rangle$, this transformation implies several operations including complex conjugation, and inversions $n\to -n$.

In that case the Floquet operator possesses the property

$$U(T,t_0) \equiv U(T,t_0)^{\Xi},$$

whose matrix elements obey

$$[U(T,t_0)]_{n,m} = [U(T,t_0)^{\Xi}]_{n,m} = [U(T,t_0)]_{-n,-m}.$$

The latter relation holds whenever the transformation is done around the symmetric points, namely $t_0=t_s$.

Let us analyze the symmetry

$$S_a: t \to t + T/2, \quad x \to -x.$$

This corresponds to the transformation

$$t \to t + T/2, \quad n \to -n.$$

For the Floquet operator we get

$$U(T,0) \equiv U(T,T/2)U(T/2,0) \equiv [U(T/2,0)^{\Xi}]^{\mathsf{T}}U(T/2,0). \tag{C1}$$

This implies that

$$U \to U^{\Xi\mathsf{T}},$$

or, equivalently,

$$[U(T,t_0)]_{n,m} = \left[[U(T,t_0)^{\Xi}]^T\right]_{n,m} = [U(T,t_0)]_{-n,-m}.$$

APPENDIX D: ASYMPTOTIC CURRENT

The asymptotic current can be defined as follows:

$$J = \lim_{\mu\to\infty}\frac{1}{\mu}\sum_{m=1}^{\mu}\langle\psi(mT)|\hat{p}|\psi(mT)\rangle_T = \lim_{\mu\to\infty}\frac{1}{\mu}\sum_{m=1}^{\mu}\langle\langle p(mT)\rangle\rangle_T. \tag{D1}$$

The wave function can be expanded over Floquet states as

$$|\psi(t)\rangle = \sum_{\alpha} C_\alpha|\psi_\alpha\rangle. \tag{D2}$$

Similarly, one can expand the Floquet states over the plane wave function

$$|\psi_\alpha(t)\rangle = \sum_n b_{\alpha,n}|n\rangle. \tag{D3}$$

Starting from an initial plane wave $|0\rangle$, the coefficients become $C_\alpha=b_{\alpha,0}$. In such a case we get

$$\langle p(mT)\rangle = \sum_{\alpha,\alpha'} b_{\alpha,0}b^*_{\alpha',0}e^{-im(E_\alpha-E_{\alpha'})}\langle\psi_{\alpha'}|\hat{p}|\psi_\alpha\rangle. \tag{D4}$$

It was shown for chaotic systems [36] that, as the time goes on, nonlinear interference terms accumulate large and larger phases, namely $m(E_\alpha-E_{\alpha'})$. Finally, for long enough times, contributions to the directed transport are only given by diagonal terms,

$$J = \left\langle \sum_\alpha |b_{\alpha,0}|^2\langle\psi_\alpha|\hat{p}|\psi_\alpha\rangle \right\rangle_T. \tag{D5}$$

[1] P. Hänggi and R. Bartussek, Lect. Notes Phys. **476**, 294 (1996).

[2] F. Jülicher, A. Ajdari, and J. Prost, Rev. Mod. Phys. **69**, 1269 (1997).

[3] P. Reimann and P. Hänggi, Appl. Phys. A: Mater. Sci. Process. **75**, 169 (2002); P. Reimann, Phys. Rep. **361**, 57 (2002).

[4] R. D. Astumian and P. Hänggi, Phys. Today **55**(11), 33 (2002).

[5] P. Hänggi, F. Marchesoni, and F. Nori, Ann. Phys. **14**, 5170

(2005).
[6] B. Norden, Y. Zolotaryuk, P. L. Christiansen, and A. V. Zolotaryuk, Phys. Rev. E **65**, 011110 (2002).
[7] P. Reimann, M. Grifoni, and P. Hänggi, Phys. Rev. Lett. **79**, 10 (1997).
[8] I. Goychuk, M. Grifoni, and P. Hänggi, Phys. Rev. Lett. **81**, 649 (1998); **81**, 2837(E) (1998).
[9] I. Goychuk and Hänggi, Europhys. Lett. **43**, 503 (1998).
[10] J. Lehmann, S. Kohler, P. Hänggi, and A. Nitzan, Phys. Rev. Lett. **88**, 228305 (2002); M. Grifoni, M. S. Ferreira, J. Peguiron, and J. B. Majer, *ibid.* **89**, 146801 (2002).
[11] J. Gong, D. Poletti, and P. Hänggi, Phys. Rev. A **75**, 033602 (2007).
[12] C. Mennerat-Robilliard, D. Lucas, S. Guibal, J. Tabosa, C. Jurczak, J. Y. Courtois, and G. Grynberg, Phys. Rev. Lett. **82**, 851 (1999); P. Sjölund, S. J. H. Petra, C. M. Dion, S. Jonsell, M. Nylen, L. Sanchez-Palencia, and A. Kastberg, *ibid.* **96**, 190602 (2006).
[13] S. Flach, O. Yevtushenko, and Y. Zolotaryuk, Phys. Rev. Lett. **84**, 2358 (2000).
[14] O. Yevtushenko, S. Flach, Y. Zolotaryuk, and A. A. Ovchinnikov, Europhys. Lett. **54**, 141 (2001).
[15] S. Denisov, S. Flach, A. A. Ovchinnikov, O. Yevtushenko, and Y. Zolotaryuk, Phys. Rev. E **66**, 041104 (2002).
[16] H. Schanz, M.-F. Otto, R. Ketzmerick, and T. Dittrich, Phys. Rev. Lett. **87**, 070601 (2001); H. Schanz, T. Dittrich, and R. Ketzmerick, Phys. Rev. E **71**, 026228 (2005).
[17] I. Goychuk and Hänggi, J. Phys. Chem. B **105**, 6642 (2001).
[18] M. Schiavoni, L. Sanchez-Palencia, F. Renzoni, and G. Grynberg, Phys. Rev. Lett. **90**, 094101 (2003); P. H. Jones, M. Goonasekera, and F. Renzoni, *ibid.* **93**, 073904 (2004); R. Gommers, S. Bergamini, and F. Renzoni, Phys. Rev. Lett. **95**, 073003 (2005); R. Gommers, S. Denisov, and F. Renzoni, *ibid.* **96**, 240604 (2006).
[19] J. Dalibard and C. Cohen-Tannoudji, J. Opt. Soc. Am. B **6**, 2023 (1989); P. J. Ungar *et al.*, *ibid.* **6**, 2058 (1989).
[20] L. Guidoni and P. Verkerk, J. Opt. B: Quantum Semiclassical Opt. **1**, R23 (1999); W. K. Hensinger *et al.*, *ibid.* **5**, R83 (2003).
[21] T. S. Monteiro, P. A. Dando, N. A. C. Hutchings, and M. R. Isherwood, Phys. Rev. Lett. **89**, 194102 (2002).
[22] J. B. Gong and P. Brumer, Phys. Rev. Lett. **97**, 240602 (2006); J. B. Gong and P. Brumer, Phys. Rev. E **70**, 016202 (2004).
[23] M. Grifoni and P. Hänggi, Phys. Rep. **304**, 279 (1998).
[24] When calculating Husimi distributions, average kinetic energies, etc., we used the inverse gauge transformation in order to return to the original wave function.
[25] K. Husimi, Proc. Phys. Math. Soc. Jpn. **22**, 264 (1940); K. Takahashi and N. Saiton, Phys. Rev. Lett. **55**, 645 (1985).
[26] We introduced a summation by pairs in order to avoid an "oscillating" behavior of P_α for large values of α [see Eq. (20)].
[27] G. M. Zaslavsky, *Physics of Chaos in Hamiltonian Systems* (Imperial College Press, London, 1998).
[28] S. Denisov and S. Flach, Phys. Rev. E **64**, 056236 (2001).
[29] R. Graham and J. Keymer, Phys. Rev. A **44**, 6281 (1991).
[30] D. Farrelly and J. A. Milligan, Phys. Rev. E **47**, R2225 (1993); R. Utermann, T. Dittrich, and P. Hänggi, *ibid.* **49**, 273 (1994).
[31] J. Dorignac and S. Flach, Phys. Rev. B **65**, 214305 (2002).
[32] F. Haake, *Quantum Signature of Chaos* (Springer-Verlag, London, 1991).
[33] G. Ritt, C. Geckeler, T. Salger, G. Cennini, and M. Weitz, Phys. Rev. A **74**, 063622 (2006).
[34] M. Latka, P. Grigolini, and B. J. West, Phys. Rev. A **50**, 1071 (1994).
[35] G. Casati, B. Chirikov and L. Shepelyansky, Phys. Rep. **154**, 77 (1987).
[36] H. Lignier, J. C. Carreau, P. Szriftgiser, and D. Delande, Europhys. Lett. **69**, 327 (2005).